Role of Intervening Mg II Absorbers on the Rotation Measure and Fractional Polarization of the Background Quasars

Sunil Malik[1] , Hum Chand[2,3], and T. R. Seshadri[1]

[1] Department of Physics and Astrophysics, University of Delhi, Delhi-110007, India; sunilmalik1993@gmail.com
[2] Aryabhatta Research Institute of Observational Sciences (ARIES), Manora Peak, Nainital-263002, India
[3] Department of Physics and Astronomical Sciences, Central University of Himachal Pradesh (CUHP), Dharamshala-176215, India

Abstract

We probed the magnetic fields in high-redshift galaxies using excess extragalactic contribution to residual rotation measure (RRM) for quasar sightlines with intervening Mg II absorbers. Based on a large sample of 1132 quasars, we have computed RRM distributions broadening using median absolute deviation from the mean ($\sigma_{\rm rrm}^{\rm md}$), and found it to be 17.1 ± 0.7 rad m^{-2} for 352 sightlines having Mg II intervening absorbers in comparison to its value of 15.1 ± 0.6 rad m^{-2} for 780 sightlines without such absorbers, resulting in an excess broadening ($\sigma_{\rm rrm}^{\rm ex}$) of 8.0 ± 1.9 rad m^{-2} among these two subsamples. This value of $\sigma_{\rm rrm}^{\rm ex}$, has allowed us to constrain the average strength of magnetic field (rest frame) in high-redshift galaxies responsible for these Mg II absorbers, to be $\sim 1.3 \pm 0.3$ μG at a median redshift of 0.92. This estimate of magnetic field is consistent with the reported estimate in earlier studies based on radio-infrared correlation and energy equipartition for galaxies in the local universe. A similar analysis on subsample split based on the radio spectral index, α (with $F_\nu \propto \nu^\alpha$), for flat ($\alpha \geqslant -0.3$; 315 sources) and steep ($\alpha \leqslant -0.7$; 476 sources) spectrum sources shows a significant $\sigma_{\rm rrm}^{\rm ex}$ (at 3.5σ level) for the former and absent in the latter. An anticorrelation found between the $\sigma_{\rm rrm}^{\rm md}$ and percentage polarization (p) with a similar Pearson correlation of -0.62 and -0.87 for subsamples with and without Mg II, respectively, suggests the main contribution for decrements in the p value to be intrinsic to the local environment of quasars.

Unified Astronomy Thesaurus concepts: Magnetic Fields (994); Quasars (1319); Galaxies (573); Extragalactic astronomy (506)

Supporting material: machine-readable tables

1. Introduction

Magnetic field has a significant impact on several astrophysical processes such as transport and confinement of cosmic rays, star formation in the galaxy, cloud collapse, and galactic outflows (e.g., Mestel & Paris 1984; Rees 1987; Watson & Perry 1991; Vacca et al. 2018). Several probes, such as synchrotron radiation, Faraday rotation (FR), Zeeman splitting, dust polarization, and dust emission, are available for investigating it at different length scales. Among them, FR is a powerful probe to study the strength of the line-of-sight component of the magnetic field over cosmic distances (e.g., Kronberg & Simard-Normandin 1976; Kronberg et al. 1977, 2008; Kronberg & Perry 1982; Welter et al. 1984; You et al. 2003; Beck et al. 2005; Bernet et al. 2008, 2010, 2012; Hammond et al. 2012; Bhat & Subramanian 2013). FR is quantified by the observed rotation measure (RM) which for a radio source at emission redshift, $z_{\rm emi}$, is given by,

$$\mathrm{RM}(z_{\rm emi}) = 8.1 \times 10^5 \int_{z_{\rm emi}}^{0} \frac{n_e(z) B_\parallel(z)}{(1+z)^2} \frac{dl}{dz} dz. \quad (1)$$

Here, RM is measured in units of rad m^{-2}, n_e is the number density of electron (in cm^{-3}), $B_\parallel$ is the longitudinal magnetic field component (measured in Gauss), and dl/dz is the column length (in parsecs) per unit redshift interval.

The total RM can be expressed as a sum of the following four components:

$$\mathrm{RM} = \mathrm{RM}_{\rm QSO} + \mathrm{RM}_{\rm IGM} + \mathrm{RM}_{\rm abs} + \mathrm{GRM}. \quad (2)$$

Here, $\mathrm{RM}_{\rm QSO}$ is the intrinsic contribution due to the source (i.e., the quasar) itself, $\mathrm{RM}_{\rm abs}$ denotes the contribution to RM of any intervening galaxy which happens to be in the line of sight, GRM refers to the galactic RM by our galaxy Milky Way, and $\mathrm{RM}_{\rm IGM}$ is the contribution by the intergalactic medium (IGM) which is likely to be negligible as compared to that of the other three components.

To study the extragalactic contribution, GRM is a contamination and needs to be removed. On doing this we are left with the residual rotation measure (RRM) given by,

$$\mathrm{RRM} = \mathrm{RM} - \mathrm{GRM}. \quad (3)$$

Further, distribution of RRM in our sample can be divide into two subsamples, one consisting of sightlines with absorption due to one or more intervening galaxies, detected in the form of Mg II absorption systems (i.e., $\mathrm{RM}_{\rm QSO} + \mathrm{RM}_{\rm IGM} + \mathrm{RM}_{\rm abs}$), and the other without any such absorption systems (i.e., $\mathrm{RM}_{\rm QSO} + \mathrm{RM}_{\rm IGM}$). The statistical properties of RRM in these two subsamples, or more specifically the difference among them, can be a unique tool to probe the global properties of the magnetic fields at high-redshift galaxies (e.g., Oren & Wolfe 1995; Bernet et al. 2008, 2010, 2012, 2013; Kronberg et al. 2008; Hammond et al. 2012; Bhat & Subramanian 2013; Joshi & Chand 2013; Farnes et al. 2014b; Mao et al. 2017; Basu et al. 2018).

For instance, the study by Bernet et al. (2008) used high-resolution spectra of 76 quasars and showed that quasar spectrum observations containing strong Mg II systems are associated with the larger RRM values at a wavelength of 6 cm. Subsequently, Bernet et al. (2010) showed that such an association of larger RRM exists only for Mg II absorbers having rest frame equivalent width (EW$_r$) > 0.3 Å, and is absent for absorbers with EW$_r$ ⩽ 0.3 Å. This was further

supported by the investigation of Bernet et al. (2013) where they found that sightlines with Mg II systems having impact parameter <50 kpc indeed have higher RM as compared to those with Mg II absorbers at a higher impact parameter. Another technique to measure RRM based on the radio-synthesis method has been used by Kim et al. (2016) which confirms that intervening systems are strongly associated with depolarization.

Similarly, the statistical properties such as broadening of RRM distribution at different redshift bins have been used to infer the redshift evolution of cosmic magnetic field (e.g., see Welter et al. 1984; Watson & Perry 1991; Kronberg et al. 2008; Arshakian et al. 2009; Bernet et al. 2012; Hammond et al. 2012; Neronov et al. 2013; Rodrigues et al. 2019). For instance, Kronberg et al. (2008) used 268 sightlines with RM measurements at a wavelength of ~10 cm in their analysis and found that the distribution of RMs broadened with redshifts. However, Hammond et al. (2012), did not find any such redshift evolution though they used a larger sample of 3650 quasars with RM compiled using a catalog of Taylor et al. (2009), based on NRAO VLA SKY SURVEY (NVSS) at a wavelength of 21 cm. This lack of firmness could be due to the fact that the sample used in this study is a mixture of sightlines with and without intervening absorbers. Since different intervening absorbers can have different absorption redshifts, they may alter their analysis of RRM pattern which is probed with various emission redshift bins of the background polarized quasars.

In an attempt to understand this discrepancy, Bernet et al. (2012) also analyzed the data set of Taylor et al. (2009) based on NVSS radio data at 21 cm, where they had separated the sightlines with and without intervening absorbers. They compared their results with the work of Kronberg et al. (2008) and Hammond et al. (2012) who also used the RM values at a wavelength of 21 cm, and with that of Bernet et al. (2008, 2010) who used RM values at a wavelength of 6 cm. They too did not find either an increase of the RM standard deviation (SD) with redshift or any correlation of RM strength with Mg II absorption lines contrary to the result at 6 cm by Bernet et al. (2008, 2010). To reconcile this discrepancy, they have proposed an inhomogeneous Faraday screen model due to the intervening absorbers/galaxies which dilute the RRM contribution at 21 cm more as compared to that at the wavelength of 6 cm. Later, Joshi & Chand (2013) investigated the dependence of RRM at 21 cm on intervening absorption systems with an enlarged sample consisting of 539 quasars separated out in the subsamples with and without Mg II absorbers. In their study, they found that SD of RRM ($\sigma_{\rm rrm}$) at 21 cm and the presence of Mg II absorbers are correlated though only at about 1.7σ level, and hence at a lesser confidence level as compared to the above studies at the wavelength of 6 cm (though using relatively smaller sample).

As an alternative route to understand the above discrepancy in the correlation of $\sigma_{\rm rrm}$ vis-a-vis presence of Mg II absorbers at wavelength of 21 and 6 cm, Farnes et al. (2014b) explored the effect of apparent frequency-dependent observational selection bias. This could arise because one may select different source populations, with different morphology and positions in relation to the optical counterparts at these high and low radio frequencies. They used the spectral index as a criterion to split their sample of 599 sources (having optical

spectra, RM, and spectral slope) into flat-spectrum and steep-spectrum subsamples. In their analysis, they found that the flat-spectrum subsample shows significant correlation (at ~3.5σ level) between the presence of Mg II absorption and RM measurement at ~21 cm, while that corresponding to the subsample of steep-spectrum sources do not show any such correlation.

Apart from the RRM measurement for these quasar sightlines, their observed fractional polarization (p) is another parameter that might also be a useful tool to probe the magnetic field in the intervening galaxies, again by comparing p values and its correlation with RRM for subsamples with and without Mg II absorbers. Many past studies have explored this possibility and have found that indeed higher RRM is associated with the lesser p value (Hammond et al. 2012; Bernet et al. 2013; Kim et al. 2016). For instance, Hammond et al. (2012) found an anticorrelation between RRM and fractional polarization. One possible physical bias suggested by them was the presence of intervening absorbers, which have a mixture of sightlines with and without the Mg II absorbers, recalling the fact that RM distribution is used in their study.

It is evident from the abovementioned studies that while using the RM to understand the magnetic field of the high-z galaxies and their evolution, it is important to remove various degeneracies in the observed RM values caused by different contributions (e.g., see Equation (2)). This necessitates the splitting of the sample into various subsamples based on either the radio spectral slope and/or the presence/absence of the intervening absorbers. However, as pointed out above, such splitting will also lead to a small statistical problem which may not allow one to draw any firm conclusion on the nature of the magnetic field based on RM studies. It may be noted that the main hindrance in improving the sample size in such studies is the scarcity of the optical spectra for the sample having RM measurements, which is very crucial to separate out quasar sightlines with and without the intervening galaxies that are revealed as the intervening Mg II absorbers.

However, with the advent of the large spectroscopic survey such as Sloan Digital Sky Survey (SDSS) Data Release (DR)-7, 9, 12, and 14, it has now become possible to enlarge the RM sample for which optical spectra is available. At the same time, large radio catalogs of RM such as that compiled by Taylor et al. (2009) consisting of RM measurements of 37,453 sources are now available. One also has radio spectral slope compilation such as that by Farnes et al. (2014a) consisting of 25,649 sources. It is useful to cross-correlate these optical catalogs with these large radio catalogs of RM. This forms the main motivation of our work in this paper in which we have doubled the sample size by including the abovementioned recent SDSS DRs. We split the sample into subsamples based on the radio spectral slope and/or the presence/absence of the intervening absorbers. Such enlarged samples will be very useful (i) to quantify the role of intervening galaxies and their equivalent widths on RRM by comparing subsamples with and without intervening absorbers, along with their subsamples such as steep and/or flat-spectrum radio quasars, (ii) probe any redshift evolution of RRM, and (iii) search for any effect of the intervening absorbers on the percentage polarization of the background quasars, so as to finally infer the presence and strength of magneto-active plasma in these high-redshift galaxies.

Table 1
Details About Our Selection of 1135[d] Quasars Sample

Criteria	DR7	DR9	DR12	DR14
Total	84533	15439	297301	525982
z-range[a]	75450	7640	148871	285042
TSS09-match[b]	673	51	404	588
Taken[c]	673	23	257	182

Notes.
[a] $0.38 \leqslant z_{emi} \leqslant 2.3$, based on SDSS spectral coverage.
[b] Number of sources found to be common within $7''$ between various SDSS data releases and the TSS09 RM catalog consisting of RM values for 37,543 sources.
[c] The number of sources taken from the cross-match found for our sample, after removal of any repeated sources among the above SDSS data release.
[d] Also included three outlier $>9\sigma$, our final sample consists of 1132 sources (e.g., Table 2).

This paper is organized as follows. We discuss in Section 2 the sample selection which we assembled from several optical and radio catalogs. In Section 3 we present the method of classification of sightlines based on detection of Mg II systems. We present our analysis and results in Section 4. Discussion of our major findings and conclusions are presented in Section 5.

2. The Sample

For RM measurement of quasars, we have used the catalog of Taylor et al. (2009, henceforth TSS09)[4] consisting of RM values for 37,543 sources based on NVSS observations. In the catalog they used Q and U Stokes parameters in two frequency bands, 1.36 and 1.43 GHz, to estimate the polarized intensity and percentage polarization.

For searching the optical counterpart of the quasars listed in TSS09, we have used SDSS DR-7, 9, 12, and 14 catalogs of quasars for their optical spectra by putting a constraint on emission redshift (z_{emi}) of sources to be in a range $0.38 \leqslant z_{emi} \leqslant 2.3$. Here, the upper redshift cutoff of 2.3 is imposed based on the upper limit of 9000 Å on the wavelength of the SDSS spectrum. For quasars with redshift more than this limit, the Mg II emission lines is beyond the SDSS spectral coverage. Hence, our upper limit avoids the ambiguity of any Mg II absorber falling above the spectral coverage. Our lower limit of 0.38 on the emission redshift ensures that the starting observed wavelength of SDSS spectra at 3800 Å allows us to detect at least one Mg II doublet, if present. Further, we cross-correlate the RM catalog of TSS09 with all the quasars (i.e., from the SDSS DR-7, 9, 12, and 14 catalogs) fulfilling the above redshift criterion (i.e., $0.38 \leqslant z_{emi} \leqslant 2.3$), by demanding that their optical and radio positions match within an offset of less than $7''$. This optimal offset of $7''$ was chosen based on the analysis of Singh & Chand (2018), where they showed that at NVSS resolution this degree of tolerance is optimal in such a cross-correlation with optical positions of SDSS catalogs.

The details of the outcome of our above cross-correlation among these catalogs are given in Table 1.

As can be seen from this table (last row), after removal of the quasar duplications among various DRs of SDSS, the SDSS DR-7, 9, 12, and 14 have contributed 673, 23, 257, and 182 quasars, respectively, leading to the merged sample of 1135

sources. In fact, we also note here that Xu & Han (2014) have also complied RM data for 4553 sources using observations in the frequency range from 1.3 to 2.3 GHz. However, to avoid the inhomogeneity due to the mixing of two catalog, we have only used the (larger) catalog TSS09 as our reference catalog for RM measurement. By not using the sample of Xu & Han (2014), only nominal decrements of about 2.7% occur in our final sample size.

Further, we have noted that in the catalog of TSS09 based on NVSS the value of GRM is not available. Hence, we have made use of the GRM compilation by Xu & Han (2014) based on their online GRM calculator.[5] Out of the total of 1135 sources selected by us, 134 sources were common with Xu & Han (2014) and hence we could use the GRM values for them directly from this catalog. For the remaining 1001 sources, the above online GRM calculator has been used to estimate their GRM values. Here, we have assumed that the error in GRM due to the difference in the measurement frequency (1.3–2.3 GHz in the Xu & Han (2014) and 1.4 GHz in the TSS09) is negligible as compared to the typical uncertainty in the GRM measurements themselves.

The fraction of our sources with |RRM| values $\leqslant 25$, 50, and 100 rad m^{-2} is typically found to be 81.89%, 96.11%, and 99.55%, respectively. In this distribution, we noted three outliers in RRM with values of 142.4 (SDSS J012142+114950), −473.8 (SDSS J111857+123442), and −172.1 rad m^{-2} (SDSS J110120 +415308) which deviate from the mean at a more than 9σ level. In order to avoid the dominance of these outliers especially on the mean and SD we have excluded them from our analysis and hence we are left with 1132 sources for our final analysis, with their details as given in Table 2.

3. Identification of Mg II Systems

The identification of the Mg II absorption doublet in the normalized continuum spectrum was carried out using the procedure discussed in detail by Joshi & Chand (2013; see also Mishra et al. 2018). Briefly, the procedure automatically searches for absorption features in the normalized spectrum in the range $(1 + z_{emi}) \times 1216 < \lambda < (1 + z_{emi}) \times 2803$ Å. A search was carried out of such individual sightline for absorption features, fitted with a Gaussian profile by taking an initial full width at half maximum of 2.5 pixels. Out of all probable cases, the selection was made by accepting only the lines with line depth (i.e., at centroid) above three times the error bar in that region of the spectrum. The absorption features thus identified for each quasar were searched for absorption line pairs. For this purpose, in our procedure we first computed the redshift of a given absorption feature, assuming it to be Mg IIλ2796. The corresponding positions of the expected Mg IIλ2803 and Fe IIλ2600 lines were then inspected visually in their velocity plots. Here, we have also used the line profile matching technique of the doublet. For this, we first plotted the normalized spectrum around the candidate Mg II doublet and then overplotted the same spectrum by shifting the wavelength axis by a factor of Mg IIλ 2796.3543/Mg IIλ 2803.5315 (i.e., 0.997). The location of reasonable overlap between the absorption lines in the shifted and the original (unshifted) spectra were marked as a detected Mg II absorption system.

---

[4] http://www.ucalgary.ca/ras/rmcatalogue

[5] http://zmtt.bao.ac.cn/RM/searchGRM.html

Table 2
Main Properties of our 1132 Quasars Sample (After Discounting Three Outliers at the 9σ Level)

SDSS Name	RM	δRM	GRM	δGRM	RRM	δRRM	n(Mg II)	z_{emi}	p	δp	α[a]
			(rad m^{-2})						(%)	(%)	
(1)	(2)	(3)	(4)	(5)	(6)	(7)	(8)	(9)	(10)	(11)	(12)
J142746+002848	25.3	13.6	3.9	6.1	21.4	14.9	0	1.2628	5.97	0.3	- - - -
J003936+204912	−23.3	6.5	−24.4	8.2	1.1	10.5	0	1.3778	3.07	0.1	−0.77
J095443+403636	−3.1	3.8	−1.0	4.2	−2.1	5.6	1	0.7821	5.53	0.1	−0.97
J083824+123000	30.8	9.4	29.8	7.3	1.0	11.9	2	1.6221	3.75	0.2	−0.96
...	...	...	...	...	...	...	...	...	...	...	...

Notes.

[a] Radio spectral indices, α define by $F_\nu \propto \nu^\alpha$ has been taken from Farnes et al. (2014a).

(This table is available in its entirety in machine-readable form.)

For each detected Mg II absorption system, we also assessed the quality of our underlying continuum fit during our visual check. If deemed desirable we carried out a local continuum fitting and this improved fit was then used to obtain a better estimate of equivalent width of Mg II lines. Out of total 1132 sightlines in our sample we found that 352 quasar sightlines have at least one Mg II absorber and the remaining 780 quasar sightlines are without any such Mg II absorbers. Among the 352 sightlines, 278 have one absorber each, 63 have two absorbers each, and 11 have more than two absorbers, resulting in a total detection of 442 Mg II absorption systems, as listed in Table 3 along with details of their z_{emi}, z_{abs}, and EW$_r$. In Figure 1 we show the plot of RRM versus z_{emi} for sightlines without intervening absorbers, (i.e., n(Mg II) = 0) and RRM versus z_{abs} for sightlines with n(Mg II) > 0 along with their histograms (e.g., see the right, upper side of the plots). As can be noted from the RRM histogram plot, a Gaussian fit (using rms minimization) describes RRM distribution reasonably well both for subsamples with and without Mg II absorbers. We will be using this aspect while computing the difference of SD (in quadrature, e.g., see Equation (7)) among the sightlines with and without Mg II systems.

We also noted here that the compilation of Mg II systems for all the quasars belonging to SDSS DR-7, 9 is also reported by Zhu & Ménard (2013, henceforth ZM13), for DR-12 by using their online catalog[6] (henceforth ZM17) and for SDSS DR-14 by Raghunathan et al. (2016, henceforth RS16). However, for the sake of uniformity in identifying the Mg II system among the members of our sample belonging to the various above-mentioned SDSS DRs, and also due to the importance of the visual check (e.g., for profile matching and continuum errors) as outlined above, our analysis relies on our own Mg II system identification. This is particularly important as the lack of a visual check might not have effect on analysis using few thousands of sightlines (e.g., in ZM13, ZM17, and RS16), but may have a significant impact in the analysis like in this study where only a few hundred quasars contribute in a subsample. Just for comparison we noticed that the ZM13, ZM17, and RS16 catalog (based on automated search) missed genuine 27, 31, and 17 Mg II systems, respectively. On the other hand the number of false detections found were 10, 5, and 2 Mg II systems, respectively. The difference is only about ∼8%. However, it can still significantly affect the RRM analysis which also illustrates the importance of supplementing the automated Mg II search by the visual check as adopted in our procedure of Mg II identification.

Table 3
Main Properties of Our 442 Mg II Absorption Systems Seen Toward 352 Quasar Sightlines in Our Sample

SDSS Name	z_{emi}	z_{abs}	EW$_r$(Å)	δEW$_r$(Å)
(1)	(2)	(3)	(4)	(5)
J095443+403645	0.7821	0.742	0.63	0.09
J024534+010814	1.5296	1.113	1.77	0.17
J003032−021156	1.8048	1.372	1.71	0.08
J003032−021156	1.8048	1.454	1.25	0.10
...	...	...	...	...
...	...	...	...	...

(This table is available in its entirety in machine-readable form.)

4. Analysis and Results

4.1. Comparison of RRM Distribution for Subsample with and Without Mg II Absorbers

To carry out the comparison of the RRM distribution for subsamples with and without Mg II absorbers, we have shown the cumulative probability distribution (CPDF) of their absolute value of RRM (|RRM|) in Figure 2. Usually Kolmogorov–Smirnov test (KS-test) is used in the literature to quantify any statistical difference between two such distributions. However, for distributions that differ mainly in their tailed regions, it is found that the Anderson–Darling[7] test (hereafter, AD-test) could be the preferred test instead of the KS-test. Therefore we use the AD-test throughout except while comparing with the results in the literature based on the KS-test. For the above |RRM| distributions in the subsamples with and without Mg II absorbers, the null hypothesis probability, that these two distributions are drawn from the same distribution, is found to be ∼68%. This shows that the functional form of their CPDF is almost the same. However, it can be noticed from the CPDF plots shown in the Figure 2 that these two CPDFs cross each other multiple times in the |RRM| range between 15 and 60, being smoother for the case of the subsample with n(Mg II) = 0. Such |RRM| fluctuations in the sample with n(Mg II) > 0 could also be due to the probable scatter caused by the presence of magnetic filed in the intervening galaxies responsible for the Mg II absorbers. This is over and above a possible smearing out of any difference due to the range in redshift and radio spectral indices (Sections 4.2
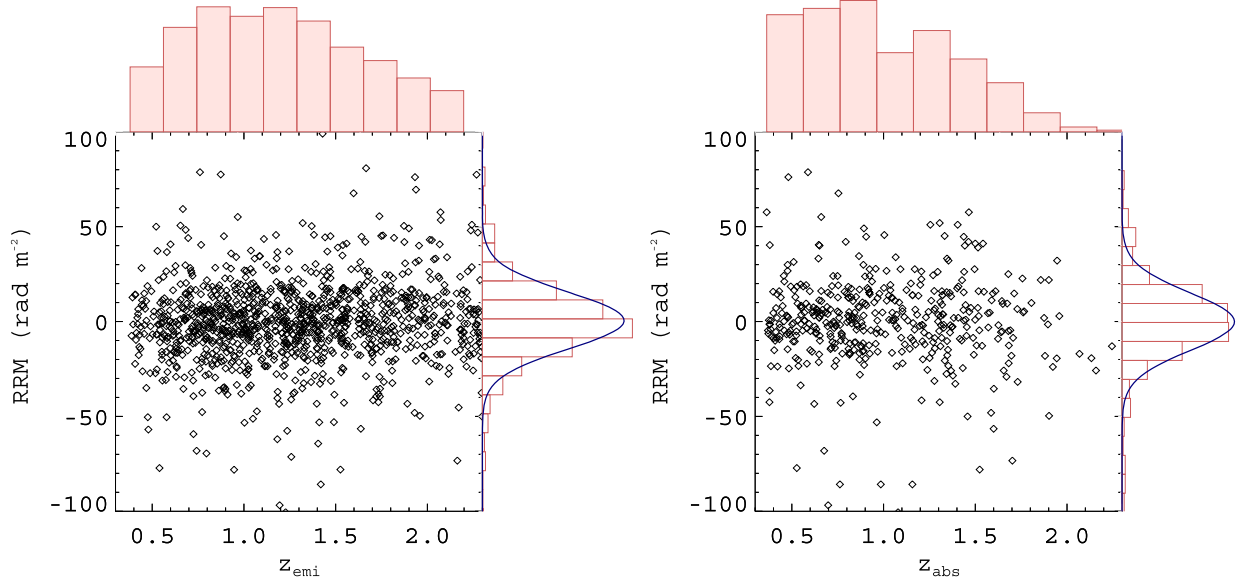
Figure 1. Left panel: the distribution of RRM (i.e., RM−GRM) with the emission redshift, z_{emi}, for the 780 sightlines with n(Mg II) = 0 along with the histogram of z_{emi} on the upper axis and histogram of RRM on the right axis, fitted (using rms minimization) with a Gaussian function (thick solid blue line). Right panel: same as left, but for 352 sightlines having n(Mg II) > 0 with absorption redshift (z_{abs}) of Mg II absorbers.
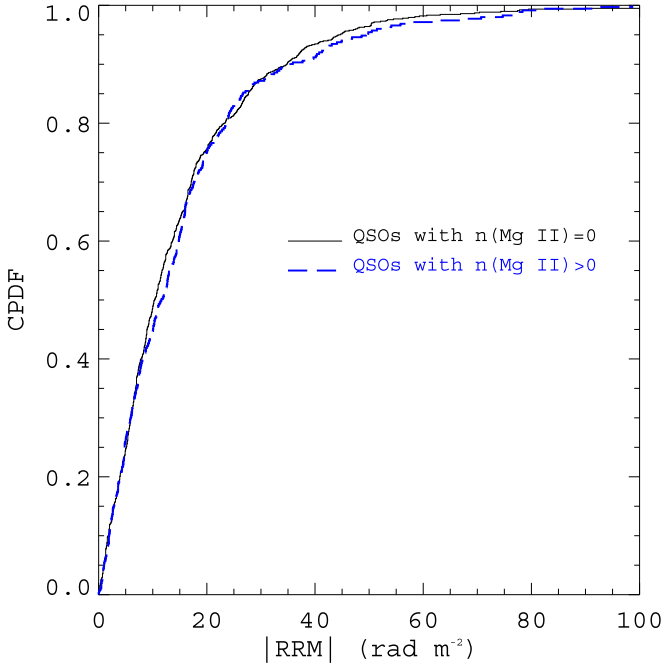

Figure 2. Cumulative probability distribution (CPDF) of the absolute value of RRM (i.e., |RRM|), for the quasar sightlines with (blue dashed line) and without Mg II absorbers (black solid line).

and 4.4). Therefore, RRM distribution being an important observational parameter, we have quantified it by measuring its broadening in the subsample with Mg II absorbers in comparison to the subsample without such absorbers (even though their CPDF form may be similar apart from scatter).

This commonly used method is to compute the SD of the subsample as,

$$\sigma_{rrm}^{sd} = \sqrt{\frac{\sum_{i=1}^{N}(x_i - \bar{x})^2}{(N - 1)}}, \qquad (4)$$

with error ($\delta\sigma_{rrm}^{sd}$) given by,

$$\delta\sigma_{rrm}^{sd} = \frac{\sqrt{\sum_{i=1}^{N}(x_i - \bar{x})^2(\delta x_i)^2 + (\overline{\sum_{i=1}^{N}(x_i - \bar{x})^2})(\delta\bar{x})^2}}{(N - 1) \times \sigma_{rrm}^{sd}}. \qquad (5)$$

Here, x_i and δx_i is the RRM measurements and error on the RRM, $\bar{x}$ and $\delta\bar{x}$ represents the mean and the error on the mean of the RRM measurements, respectively. We get the σ_{rrm}^{sd} for the subsamples with and without intervening Mg II systems, 22.9 ± 0.6 rad m^{-2} and 21.6 ± 0.4 rad m^{-2}, respectively, as listed in Table 4.

We also note that such a comparison, quantified by σ_{rrm}^{sd}, might also get dominated by the presence of a few outliers of the samples. A better alternative is to employ the median absolute deviation from the mean, MADFM (MD hereafter) rather than σ_{rrm}^{sd}, the former also being resistant to outliers and computed as:

$$\text{MADFM} = \text{Median}(|x_i - \bar{x}|). \qquad (6)$$

The MADFM can be used as a consistent estimator for the estimation of spread, analogous to σ_{rrm}^{sd}, as $\sigma_{rrm}^{md} = k \times \text{MADFM}$ with $k = 1.4826$ for normally distributed data (Leys et al. 2013). This is a reasonable approximation for our RRM distribution as revealed by the Gaussian fit of RRM shown in Figure 1, apart from the minor deviation due to Mg II systems we are searching for in the sample with Mg II absorber vis-a-vis without such absorbers. Therefore, we will be quantifying the broadening of our RRM distribution using the σ_{rrm}^{md} unless otherwise specified (e.g., when comparing with literature results based on the SD method).

We found that σ_{rrm}^{md} for subsamples with intervening absorbers (i.e., with n(Mg II) > 0) and without these absorbers (i.e., with n(Mg II) = 0) to be 17.1 ± 0.8 rad m^{-2} and 15.0 ± 0.6 rad m^{-2}, respectively (see Table 4). Here, the error bar on the MADFM value is calculated by using a standard procedure applicable for the error on a mean value of such deviations (i.e., $\langle|x_i - \bar{x}|\rangle$).

Table 4
Results of RRM Distribution for Various Subsamples

Sample Type	n(Mg II) = 0			n(Mg II) > 0			σ_{rrm}^{ex} Using MADFM/SD		$P_{null}(\%)$
	N	σ_{rrm}^{md}	σ_{rrm}^{sd}	N	σ_{rrm}^{md}	σ_{rrm}^{sd}	$\sigma_{md}^{ex}(n\sigma)$	$\sigma_{sd}^{ex}(n\sigma)$	AD[a]
Full	780	15.1 ± 0.6	21.6 ± 0.4	352	17.1 ± 0.8	22.9 ± 0.5	$8.0 \pm 1.9\ (4.2\sigma)$	$7.5 \pm 2.0(3.7\sigma)$	68
$\alpha \geqslant -0.3$[b]	204	14.3 ± 1.1	22.3 ± 0.8	111	17.3 ± 1.3	22.0 ± 1.1	$9.8 \pm 2.8(3.5\sigma)$	- - - -	24
$\alpha \leqslant -0.7$[c]	336	15.2 ± 0.9	21.7 ± 0.6	140	15.6 ± 1.2	19.4 ± 0.9	$3.4 \pm 7.2(0.5\sigma)$	- - - -	69

Notes.
[a] The percentage probability of null hypothesis using the Anderson–Darling (AD) test for a subsample with respect to the n(Mg II) = 0 subsample.
[b] Flat spectrum radio quasars.
[c] Steep-spectrum radio quasars.

To quantify the excess broadening (σ_{rrm}^{ex}) introduced by the intervening absorbers, we have subtracted in quadrature the σ_{rrm} (assuming Gaussian distribution, e.g., as shown in Figure 1) for the quasar subset with ($\sigma_{rrm(w)}$) and without ($\sigma_{rrm(wo)}$) Mg II absorber as,

$$\sigma_{rrm}^{ex} = \sqrt{\sigma_{rrm(w)}^2 - \sigma_{rrm(wo)}^2} \qquad (7)$$

and its associated error as,

$$\delta\sigma_{rrm}^{ex} = \frac{1}{\sigma_{rrm}^{ex}} \sqrt{\sigma_{rrm(w)}^2 \delta\sigma_{rrm(w)}^2 + \sigma_{rrm(wo)}^2 \delta\sigma_{rrm(wo)}^2}. \qquad (8)$$

This excess is found to be 8.0 ± 1.9 rad m^{-2} (i.e., at 4.2σ evel) and 7.5 ± 2.0 rad m^{-2} (i.e., at 3.7σ level) while estimating the broadening of the RRM using MADFM (i.e., σ_{rrm}^{md}) and SD (i.e., σ_{rrm}^{sd}) method, respectively, as listed in Table 4.

We note here that the results derived to quantify the difference between the subsample with and without Mg II absorbers, by comparing the σ's of their RRM distributions does show discrepancy vis-a-vis derived based on the estimation of null probability (using AD-test). Such discrepancy is unlikely if the true distribution of the RRM is Gaussian as we have assumed in our estimation of σ_{rrm}^{ex} based on Equation (7). One possibility to understand this discrepancy is to use both these tests on simulated data sets of RRM having Gaussian distributions. The simulated data sets for subsamples with and without Mg II systems are different in their SD which is taken from their observed values of 15.1 ± 0.6 and 17.1 ± 0.7 rad m^{-2}, respectively. We have simulated 1000 realizations of these Gaussian random distributions for the subsamples with (352 sightlines) as well as without (780 sightlines) Mg II intervening absorbers.

We have evaluated the P_{null} based on AD-test for all these 1000 simulated data sets of RRM, among systems with and without Mg II absorbers, and found that for most of the realizations ($\sim70\%$) it is less than 10%, which is much less than the P_{null} of 68% found among real data set.

This suggests that the RRM distributions in real data sets perhaps is not strictly Gaussian, which may be a reason for the above observed discrepancy between the results based on σ_{rrm}^{ex} (assuming Gaussianity of RRM distribution) and the P_{null} based on the AD-test. However, in a larger perspective and to compare our results with earlier similar studies (e.g., see Joshi & Chand 2013 and Farnes et al. 2014b) which has assumed Gaussian distribution (hence made use of Equation (7)), we here retain our result based on this technique/estimator to spot

the effect of the magnetized plasma in these absorbers on the RM of the background quasars.

Furthermore the simulated data sets can also be used to quantify any chance probability of obtaining $\sigma_{rrm}^{ex} = 8 \pm 2$ rad m^{-2} (i.e., at 4σ level), as we have explored here only limited parameter space, and effects such as the look-elsewhere effect (Gross & Vitells 2010) may also be at play. To explore any such possibility we have carried out Monte Carlo simulations (for 10^6 random realizations) of our subsample with n(Mg II) = 0 by allowing the RRM values to vary within its 1σ error bar. Then based on the distribution of the σ_{rrm}^{ex} values (as in Equation (7)) between the median value of σ for all 10^6 realizations and the values of σ corresponding to each random subsample of 352 RRM values from each realization, we noticed that the observed excess of $\geqslant 8$ rad m^{-2} (as we found in our analysis) has a by chance probability of about $\sim18\%$. This suggests that the typical confidence level of the σ_{rrm}^{ex} could be 1–2σ rather than the $\sim4\sigma$ (based on the observed 8 ± 2 rad m^{-2}).

Further, to check the impact of the strength of the absorber on RRM distributions using our 352 sightlines with intervening absorbers, we also plotted the σ_{rrm}^{sd} at different EW$_r$ bins as shown in Figure 3. For this purpose we have used the summed EW$_r$ for sightlines with multiple absorbers. Here we did not find any firm trend between σ_{rrm}^{md} with EW$_r$, but statistics with a large number of observations of such systems can provide better clarification to this correlation.

It is important to use the above estimate of excess in σ_{rrm}^{md} of the subsample with Mg II systems as compared to the subsample without such systems to get a typical estimate of the average strength of the parallel component of magnetic fields ($\langle B_\parallel \rangle$) (rest frame) in these high-z galaxies responsible for the Mg II absorption systems. For this we have used a formalism similar to that of Kronberg et al. (2008; e.g., see their Equation (15)) as,

$$\langle B_\parallel \rangle = 5.5 \times 10^{-7} \text{G} \left(\frac{1 + \langle z_{abs} \rangle}{3.5} \right)^2$$
$$\times \left(\frac{\sigma_{rrm}^{ex}}{20 \text{ rad m}^{-2}} \right) \left(\frac{N_e}{1.7 \times 10^{21} \text{cm}^{-2}} \right)^{-1}. \qquad (9)$$

Here, N_e is the column density of electrons in the intervening absorber systems with a typical value of $N_e \sim 9 \times 10^{19}$ cm^{-2} (e.g., see, Bernet et al. 2008), and $\langle z_{abs} \rangle$ is the median redshift of the absorbers. Using, $\sigma_{rrm}^{ex} = 8.0 \pm 1.9$ rad m^{-2} (using MADFM) obtained for our full sample with and without Mg II systems (e.g., see Table 4, top row), the typical value of $\langle B_\parallel \rangle$ is
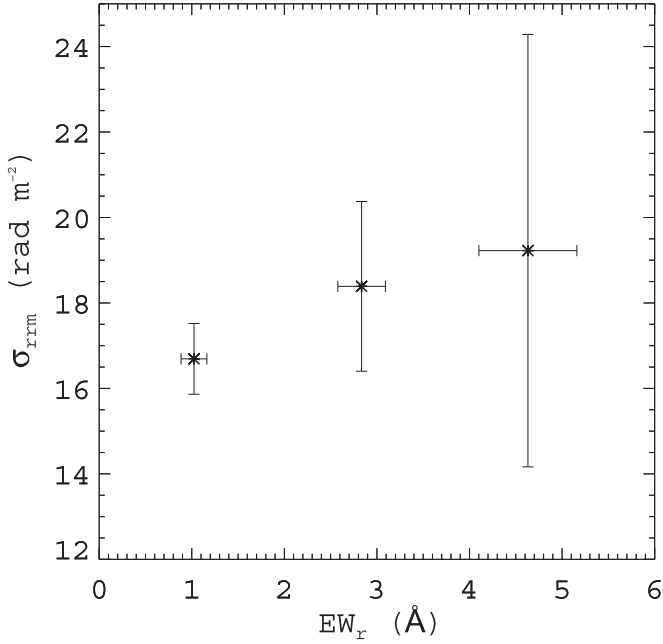
Figure 3. Plot of RRM broadening using MADFM (i.e., σ_{rrm}^{md}) in different EW_r bins, based on 352 quasars with Mg II intervening absorbers. Here, for sightlines with multiple absorbers, the EW_r of such individual sightlines has been summed up.

Figure 4. Left panel: the CPDF of |RRM| for the flat-spectrum quasar with $\alpha \geqslant -0.3$ (315 sources) for their subsamples without (black solid line) and with Mg II absorbers (blue dashed line). Right panel: same as left, but for steep-spectrum quasars with $\alpha \leqslant -0.7$ (476 sources).

found to be around $\sim 1.3 \pm 0.3\,\mu G$, in these intervening galaxies spread over the redshift range from 0.38 up to 2.24 with a median redshift of 0.92.

4.2. Correlation of RRM Using Subsamples of Flat and Steep-spectrum Sources

As pointed out by Farnes et al. (2014b), the morphology of radio sources can also introduce a bias in the correlation of RRM distribution of sightlines with Mg II absorbers, such as compact flat-spectrum sources being more aligned with the optical sightlines in comparison to the possible misalignment of lobe-dominated steep-spectrum sources. In their study, they found a significant correlation (at $\approx 3.5\sigma$ level) between the Mg II absorbers and RM in the subsample of flat-spectrum (core dominated, with $\alpha \geqslant -0.3$; for $F_\nu \propto \nu^\alpha$) sources. Such a correlation is, however, absent in the subsample of the steep-spectrum (lobe-dominated, with $\alpha \leqslant -0.7$) sources. We have also carried out an analysis similar to that in Farnes et al. (2014b) by making use of our bigger sample of 1132 sources. For the values of spectral indices, we make use of Farnes et al. 's (2014a) compilation consisting of 25,649 sources. After cross-correlating their sample with our sample of 1132 sources, we could get the α values for 1082 sources which is almost a factor of two larger than the sample of 599 sources used by Farnes et al. (2014b). Among them 476 have $\alpha \leqslant -0.7$ and 315 with $\alpha \geqslant -0.3$. The CPDFs of |RRM| for both these samples, after subclassifying them in n(Mg II) = 0 and n(Mg II) > 0 subsamples are shown in Figure 4. As can be seen from this figure, for the subclass of flat-spectrum sources, the |RRM| consistently appears to be higher for n(Mg II) > 0 in comparison to the case of n(Mg II) = 0, though the P_{null} of 24% based on the AD-test is still high. However for the subsample of steep-spectrum sources, the value of $P_{null} = 69\%$
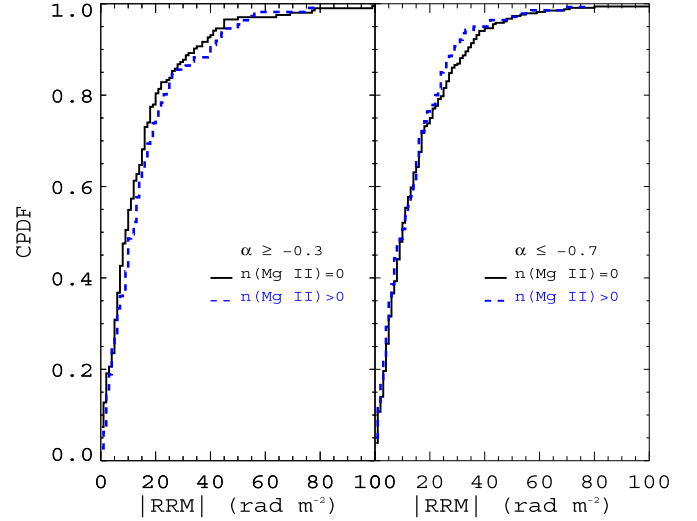
is found to be much higher though the difference is not significant.

The values of σ_{rrm}^{md}, as listed in the lower part of Table 4, is also found to be consistent with the above conclusion. The σ_{md}^{ex} of $9.8 \pm 2.8\,rad\,m^{-2}$ for flat-spectrum sources suggests the correlation at $\sim 3.5\sigma$ among the presence of Mg II absorbers and σ_{rrm}. This correlation is almost absent in the subclass of steep-spectrum sources (with excess at $\sim 0.5\sigma$ level). This result is found to be consistent with the similar 3.5σ correlation reported by Farnes et al. (2014a).

We also note that the result based on SD method for flat-spectrum sources is consistent to that derived using the MADFM, though these two methods depart for the case of subclass of steep-spectrum sources (e.g., see Table 4), perhaps due to few outlier points in this subclass. Given the fact that MADFM is more resistant to the outlier points compared to the SD, the result based on MADFM can be considered to be more robust.

4.3. Correlation of RRM with Polarization Percentage

The polarization percentage, (p), measurement were available for all our 1132 sources. To test the hypothesis that the intervening absorber might also lead to depolarization based on mechanisms such as differential Farady rotation and/or due to the beam depolarization (e.g., see Burn 1966; Sokoloff et al. 1998; Fletcher et al. 2004; Kim et al. 2016; Kierdorf et al. 2018), we first plotted the RRM versus p in the upper panel of Figure 5, which shows a trend of decrease in RRM scatter with the increase in p values. To quantify this trend we have also plotted the σ_{rrm}^{md} (based on MADFM) in various bins of p as shown in the middle panel of Figure 5. From this figure an anticorrelation between σ_{rrm}^{md} and p can be noticed in the subsample of sightlines having Mg II absorbers as well as in the subsample of sightlines without any such absorbers, with Pearson correlation coefficients, ρ_p, of -0.62 and -0.88, with significance levels of 75% and 95%, respectively. In the bottom panel of Figure 5, we have also plotted the CPDF of
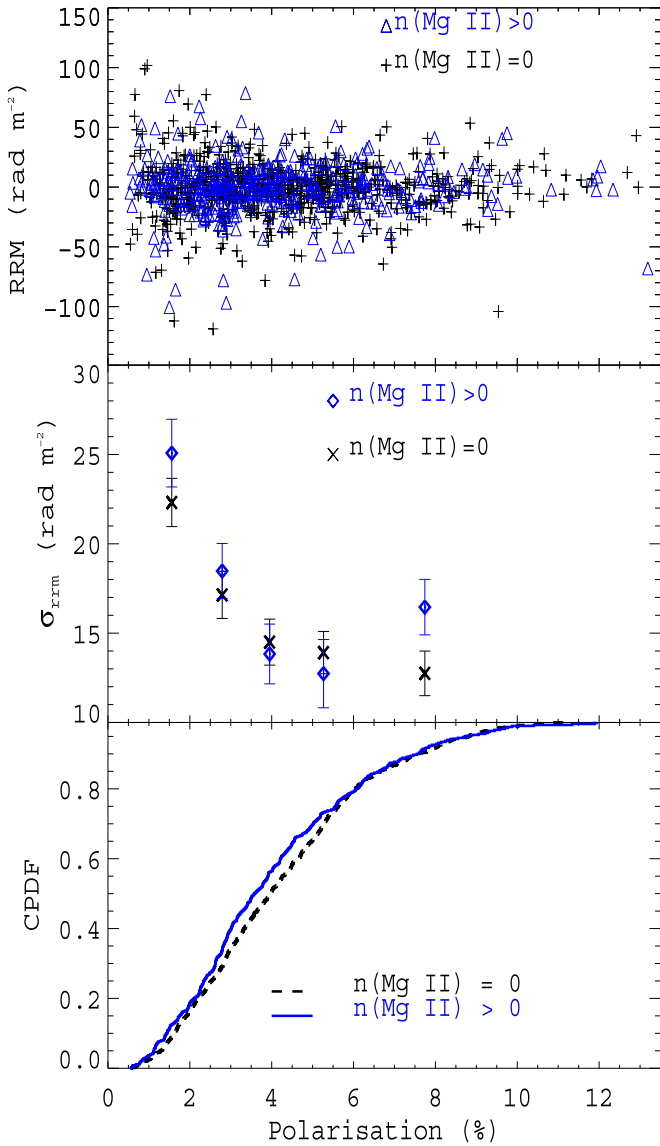
Figure 5. Upper panel: distribution of RRM with the polarization percentage, p, for sources with (blue triangle) and without (black plus) Mg II absorbers along the quasar's sightline. Middle panel: the plot of broadening of RRM (i.e., σ_{rrm}^{md}) with the polarization percentage for subsamples with (blue diamond) and without (black cross) Mg II absorbers is shown. Their values of Pearson correlation coefficient, (ρ_p) is -0.62 and -0.87, respectively. Lower panel: the CPDFs of p, for subsamples with (blue solid line) and without (black dashed line) Mg II absorbers.

Figure 6. Left panel: the CPDFs of the polarization percentage, p, for the quasars with no absorber (black line) and with absorbers (blue dotted line) for $\alpha \geqslant -0.3$. Right panel: same as the left, but for the steep-spectrum quasars sample with $\alpha \leqslant -0.7$.

polarization percentage. As can be seen from this figure, the fractional polarization for a subsample with $n(Mg\ II) = 0$ seems to be nominally higher in a systematic manner as compared to the subsample with $n(Mg\ II) > 0$. This nominal difference due to the absorbers is also revealed by the AD-test, which shows that the P_{null} among these two distributions is 12%.

Additionally, we also repeated our above analysis separately in the flat and steep-spectrum sources, by comparing their respective CPDFs of percentage polarization based on subsamples with and without Mg II absorbers as shown in Figure 6. It can be noticed from this figure that the difference (among subsamples with and without Mg II) might be more in the subclass of flat spectrum as compared to the subclass of the

steep-spectrum sources, though it is not clearly evident in either subclass. This is also corroborated by the AD-test which shows that the P_{null} is only 5% and 16% for the former and latter subclasses, respectively.

The differences between subsamples with and without Mg II absorbers not being significant (both in full as well as in subsample splitting based on spectral indices), suggest that dominant contribution toward depolarization is due to the local environment of the background quasar instead of the intervening galaxy (see also Farnes et al. 2014b).

4.4. The Redshift Evolution of RRM and Fractional Polarization

Any trend of the broadening of RRM distributions and value of polarization with the redshift could be a useful tracer of the evolution of galactic magnetic fields. For this we first plotted in Figure 7 the percentage polarization (p) verses the z_{emi}. As can be seen from this plot, z_{emi} and p seem to be uncorrelated both in the cases of subsamples with Mg II absorbers as well as the ones without. This is also evident on the basis of the over-plot of the median value of p within a bin of z_{emi} (using a bin size of ~ 0.238), which appears almost similar for subsamples with and without Mg II absorbers within the error bar. Here the error bar within the bin has been computed by the quadratic sum of two sources of errors, viz., the result of (i) individual error on p values within a bin and (ii) the statistical error computed as an rms deviation within the bin around the median value of p (i.e., $\sqrt{variance/(N-1)}$). From this figure, it is clear that as far as the value of percentage polarization and its redshift evolution is concerned the local environment dominates in comparison to the impact of intervening galaxy (if any).

Further, it is also tempting to look for any trend of σ_{rrm} and its excess at different redshift bins, as it could be a useful tracer of the evolution of galactic magnetic fields in the high-redshift galaxies. However, we noticed that with such binning in redshift space the estimate of broadening of RRM distributions could easily dominate due to the low number statistics, especially while computing the excess among subsamples with and without Mg II absorbers. As an alternative, we show in
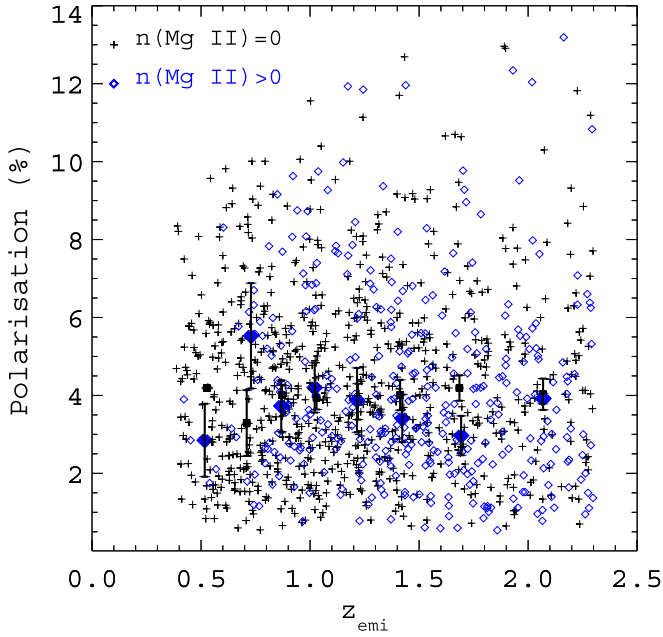
Figure 7. Distribution of polarization percentage (p) with emission redshift of the quasar, $z_{\rm emi}$, for a subsample without a Mg II absorber (black plus) and for a subsample with Mg II absorbers (blue diamond). The thick points with error bars are the corresponding median values within the redshift bins the size of 0.238.
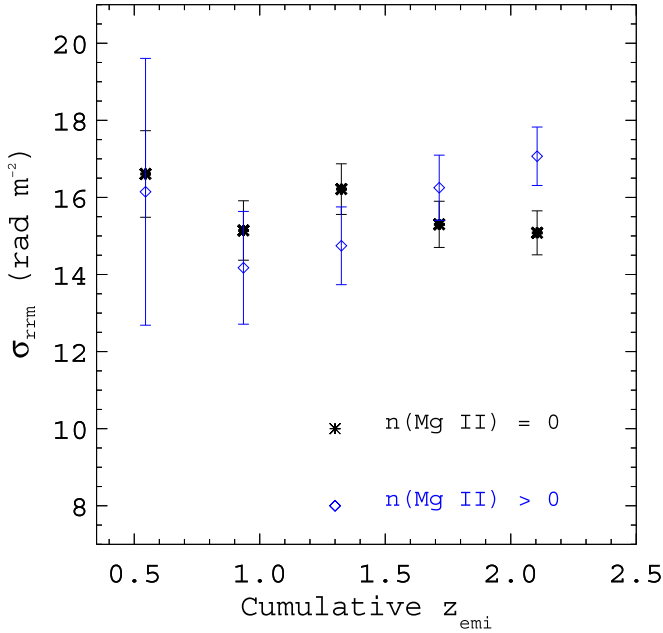

Figure 8. Plot of broadening of RRM (i.e., $\sigma_{\rm rrm}^{\rm md}$) both for subsamples with (blue diamond) and without (black star) Mg II systems in a common cumulative bins of $z_{\rm emi}$.

Figure 8 the plot of $\sigma_{\rm md}^{\rm rrm}$ over the cumulative bin of $z_{\rm emi}$, wherein the successive bin data from the higher redshift is consecutively being included to see any evolution in the $\sigma_{\rm md}^{\rm rrm}$, besides excluding the possibility of low number statistics. As can be seen from this figure, over the redshift range of 0.38–2.3 of our sample the evolution in $\sigma_{\rm md}^{\rm rrm}$ (or difference among samples in a bin with and without Mg II system) with redshift does not seem to be very strong within the error bars. Perhaps a

much larger data set may be able to distinguished any tentative difference among the two subsamples at various redshift bins.

5. Discussion and Conclusions

As pointed out in Section 1, many past studies have analyzed the impact of intervening systems on the RM distributions. Here we have carried out a similar study based on a sample size (containing 1132 sources based on SDSS 7, 9, 12, and 14) which is about twice as large as compared to previous large samples of 539 and 599 sources by Joshi & Chand (2013) and Farnes et al. (2014b; e.g., see Section 1) respectively.

Special care has been taken to separate the sightlines with and without Mg II absorbers by supplementing our automated search with a visual check of each system (see Section 3). We also employed the new method based on MADFM to compute the broadening (i.e., $\sigma_{\rm rrm}^{\rm md}$) in RRM distributions, which is found to be more resistant to the outliers as compared to the traditionally applied SD method. The excess in $\sigma_{\rm rrm}$ based on these two methods is found to be 8.0 ± 1.9 rad m^{-2} and 7.5 ± 2.0 rad m^{-2}, respectively, using the 352 sightlines with n(Mg II) > 0 and the 780 sightlines with n(Mg II) = 0. This shows that the galaxies responsible for these intervening Mg II systems do have a contribution in the RRM, which is evident at the confidence level of 4.2σ and 3.7σ based on MADFM and SD method, respectively.

Further, comparing our abovementioned 3.7σ excess, using $\sigma_{\rm rrm}^{\rm ex} = 7.5 \pm 2.0$, based on the SD method with that of the estimate of the excess of 1.7σ by Joshi & Chand (2013) using the same SD method with $\sigma_{\rm rrm}^{\rm ex} = 8.11 \pm 4.83$, implies that these are consistent with each other. This is apart from a gain in precision (about a factor of two) in our measurement mainly due to the better statistics based on our enlarged sample size (being about a factor of two larger). Similarly, an excess is also reported by many past studies (e.g., Bernet et al. 2008; Kronberg et al. 2008; Bernet et al. 2010; Farnes et al. 2014b; Mao et al. 2017).

For instance, Farnes et al. (2014b) reported an excess, based on a method of computing difference in the median value of RM distributions which is found to be 6.9 ± 1.7 rad m^{-2} (i.e., at 4σ), consistent with the trend found in our analysis. The significant excess in RRM reported by Bernet et al. (2008; see also, Bernet et al. 2010), has been arrived at by using RRM measurements at 6 cm wavelength (using 76 sources) unlike all the above studies based on RRM at 21 cm wavelength. As proposed by Bernet et al. (2012), the $\sigma_{\rm rrm}^{\rm ex}$ can be wavelength dependent with more dilution at 21 cm based on their inhomogeneous Faraday screen models. In view of the fact that we find an excess in our analysis suggests that the RRM contribution of intervening galaxies is also found to be significant at 21 cm wavelength as at 6 cm wavelength, though it can also be partly affected by a nominal contribution of the above propose inhomogeneous Faraday screen phenomena.

Additionally, similar to the Farnes et al. (2014b), we also searched for any bias due to the radio emission morphology such as compact core dominated and extended lobe-dominated sources by making a split based on their spectral index, α (where $F_\nu \propto \nu^\alpha$) namely, $\alpha \geqslant -0.3$ and $\alpha \leqslant -0.7$, respectively. As detailed in Section 4.2, we found that excess of $\sigma_{\rm rrm}$ in flat sources does indeed correlate at high significance of 3.5σ level with the presence of Mg II absorber, but such correlation is almost absent in steep-spectrum sources (see lower part of

Table 4). This is found to be consistent with that of Farnes et al. (2014b) where they have reported the $\sim 3.5\sigma$ difference. However, we also noted here that their result was based on P_{null} estimated using the KS-test by comparing the empirical cumulative-distribution functions of their two RM distributions (with and without Mg II absorbers) unlike our case where we have computed the $\sigma_{\mathrm{rrm}}^{\mathrm{ex}}$. This difference among the methods used, may also be a possible reason that in spite of the larger sample in our case the expected relative improvement in precision of the above correlation is almost similar to the relatively smaller sample (almost by factor of 2) used in the Farnes et al. (2014b) studies.

Other important additional advantages of our enlarged sample are that we could divide the sample in various bins of redshift and fractional polarization, to test any evolution of σ_{rrm} with these parameters. Our analysis indicates an anticorrelation among $\sigma_{\mathrm{rrm}}^{\mathrm{md}}$ and the fractional polarization with Pearson correlation coefficient of -0.62 and -0.87 for the subsample with and without Mg II absorbers (see Section 4.3, and Figure 5). The higher $\sigma_{\mathrm{rrm}}^{\mathrm{md}}$ found at a low fractional polarization bin might represent more randomization and hence more decrements in the fractional polarization, leading to the above observed decrements of $\sigma_{\mathrm{rrm}}^{\mathrm{md}}$ by about 10 rad m^{-2} over a range of fractional polarization from 0% to 8% (see the middle panel of Figure 5). The similarity of the anticorrelation separately in subsamples with and without Mg II absorbers shows that the intervening absorbers have negligible impact on the fractional polarization (at least in 21 cm wavelength). The impact of morphology also seems to be negligible, based on our comparison of the CPDF of subsamples with and without Mg II absorbers separately for the subclass of flat- and steep-spectrum sources (e.g., see Figure 6). The possibility of any dominant role due to the IGM based on mixing of the sources with different emission redshifts in a given polarization bin, is also unlikely as we do not see any evolution of the fractional polarization with z_{emi} both for subsamples with as well as without Mg II systems (see Figure 7). Thus our analysis suggests that the dominant factor to determine the level of polarization is based on local environment instead the intervening galaxies. This is also found consistent with the studies of Farnes et al. (2014b). However the studies by Kim et al. (2016) suggest that the intervening systems are strongly associated with depolarization, though they use a different technique of RM synthesis over a rather smaller sample size (49 unresolved quasars).

For the RRM excess $\sigma_{\mathrm{rrm}}^{\mathrm{ex}} = 8.0 \pm 1.9$ rad m^{-2} (using MADFM) obtained for our subsample with (352 sources) and without (780 sources) Mg II systems (see Table 4, top row), lead to a typical estimate of $\langle B_{\parallel} \rangle \sim 1.3 \pm 0.3\,\mu$G for the intervening galaxies responsible for these Mg II absorbers with the median redshift of 0.92 (e.g., see Section 4.1). This is found to be consistent with the recent similar estimate by Farnes et al. (2014b) of magnetic field of about $1.8 \pm 0.4\,\mu$G based on the excess of 6.9 ± 1.7 rad m^{-2} in the RM value (using 599 sources) calculated based on the difference among the median value of RM distributions. The typical value of magnetic field estimated by Bernet et al. (2008) is about 10 μG, using the RRM excess based on the RRM measurements at 6 cm (using 76 sources). Our result also supports these previous findings that a high-z galaxy contains a large enough magnetic field to be observable as a significant effect on the measured RRM value. We would like to point out that the strength of the average magnetic fields reported here is derived based on the integrated values traced by Mg II absorbers

having a range of impact parameter from the center of galaxies. Hence this should be treated as an average value of the magnetic field over the galactic scale.

On the other hand, the typical estimate of magnetic field based on the energy equipartition (pressure equilibrium) in the galactic systems also varies from 1 to 10 μG (e.g., see Beck & Krause 2005, and reference therein), by assuming the pressure balance between the cosmic rays with that of the galactic magnetic field. Similar estimates based on the radio–far-infrared correlation varied over a range of 8–23 μG in redshift up to 0.05 (e.g., see Omar & Paswan 2018) and references therein (Schleicher & Beck 2016; Basu et al. 2017; Mao et al. 2017), which are significantly higher than our estimate above based on RRM excess (i.e., $\sigma_{\mathrm{rrm}}^{\mathrm{ex}}$). However, we also note here that these studies at very low redshift consist of a relatively small sample of peculiar galaxies such as one with high star formation, etc., can perhaps have high magnetic field. This could also arise at low-z based on amplification of galactic magnetic field due to small-scale turbulent dynamo action (Bhat & Subramanian 2013; Omar & Paswan 2018). Nonetheless such an observational constraint as obtained above together with comparative studies of RRM for sightline with and without Mg II systems will prove to be important for building any model of galactic magnetism at high redshift, especially in the context of our understanding of the galaxy formation.

Further improvements on these aspects will be possible with an enlarged sample having both optical spectra as well as radio polarization measurements. Surveys, such as the square kilometer array (SKA) as well as future optical observations (of the nature of SDSS) can play crucial roles in these studies.

ORCID iDs

Sunil Malik ● https://orcid.org/0000-0003-4147-626X

References

Arshakian, T. G., Beck, R., Krause, M., & Sokoloff, D. 2009, A&A, 494, 21
Basu, A., Mao, S. A., Fletcher, A., et al. 2018, MNRAS, 477, 2528
Basu, A., Roychowdhury, S., Heesen, V., et al. 2017, MNRAS, 471, 337
Beck, R., Fletcher, A., Shukurov, A., et al. 2005, A&A, 444, 739
Beck, R., & Krause, M. 2005, AN, 326, 414
Bernet, M. L., Miniati, F., & Lilly, S. J. 2010, ApJ, 711, 380
Bernet, M. L., Miniati, F., & Lilly, S. J. 2012, ApJ, 761, 144
Bernet, M. L., Miniati, F., & Lilly', S. J. 2013, ApJL, 772, L28
Bernet, M. L., Miniati, F., Lilly, S. J., Kronberg, P. P., & Dessauges-Zavadsky, M. 2008, Natur, 454, 302
Bhat, P., & Subramanian, K. 2013, MNRAS, 429, 2469
Burn, B. J. 1966, MNRAS, 133, 67
Farnes, J. S., Gaensler, B. M., & Carretti, E. 2014a, ApJS, 212, 15
Farnes, J. S., O'Sullivan, S. P., Corrigan, M. E., & Gaensler, B. M. 2014b, ApJ, 795, 63
Fletcher, A., Berkhuijsen, E. M., Beck, R., & Shukurov, A. 2004, A&A, 414, 53
Gross, E., & Vitells, O. 2010, EPJC, 70, 525
Hammond, A. M., Robishaw, T., & Gaensler, B. M. 2012, arXiv:1209.1438
Joshi, R., & Chand, H. 2013, MNRAS, 434, 3566
Kierdorf, M., Mao, S. A., Fletcher, A., et al. 2018, arXiv:1810.03638
Kim, K. S., Lilly, S. J., Miniati, F., et al. 2016, ApJ, 829, 133

Kronberg, P. P., Bernet, M. L., Miniati, F., et al. 2008, ApJ, 676, 70
Kronberg, P. P., & Perry, J. J. 1982, ApJ, 263, 518
Kronberg, P. P., Reinhardt, M., & Simard-Normandin, M. 1977, A&A, 61, 771
Kronberg, P. P., & Simard-Normandin, M. 1976, Natur, 263, 653
Leys, C., Ley, C., Klein, O., Bernard, P., & Licata, L. 2013, J. Exp. Soc. Psychol., 49, 764
Mao, S. A., Carilli, C., Gaensler, B. M., et al. 2017, NatAs, 1, 621
Mestel, L., & Paris, R. B. 1984, A&A, 136, 98
Mishra, S., Chand, H., Krishna, G., et al. 2018, MNRAS, 473, 5154
Neronov, A., Semikoz, D., & Banafsheh, M. 2013, arXiv:1305.1450
Omar, A., & Paswan, A. 2018, MNRAS, 477, 3552
Oren, A. L., & Wolfe, A. M. 1995, ApJ, 445, 624
Raghunathan, S., Clowes, R. G., Campusano, L. E., et al. 2016, MNRAS, 463, 2640
Rees, M. J. 1987, QJRAS, 28, 197
Rodrigues, L. F. S., Chamandy, L., Shukurov, A., Baugh, C. M., & Taylor, A. R. 2019, MNRAS, 483, 2424
Schleicher, D. R. G., & Beck, R. 2016, A&A, 593, A77
Singh, V., & Chand, H. 2018, MNRAS, 480, 1796
Sokoloff, D. D., Bykov, A. A., Shukurov, A., et al. 1998, MNRAS, 299, 189
Taylor, A. R., Stil, J. M., & Sunstrum, C. 2009, ApJ, 702, 1230
Vacca, V., Murgia, M., Govoni, F., et al. 2018, Galax, 6, 142
Watson, A. M., & Perry, J. J. 1991, MNRAS, 248, 58
Welter, G. L., Perry, J. J., & Kronberg, P. P. 1984, ApJ, 279, 19
Xu, J., & Han, J. L. 2014, MNRAS, 442, 3329
You, X. P., Han, J. L., & Chen, Y. 2003, AcASn, 44, 155
Zhu, G., & Ménard, B. 2013, ApJ, 770, 130